Remote Sensing of Environment 189 (2017) 84–95

Contents lists available at ScienceDirect

Remote Sensing of Environment

journal homepage: www.elsevier.com/locate/rse

Detection of rain-on-snow (ROS) events and ice layer formation using passive microwave radiometry: A context for Peary caribou habitat in the Canadian Arctic

A. Langlois [a,b,*], C.-A. Johnson [c], B. Montpetit [a], A. Royer [a,b], E.A. Blukacz-Richards [d], E. Neave [c], C. Dolant [a,b], A. Roy [a,b], G. Arhonditsis [e], D.-K. Kim [e], S. Kaluskar [e], L. Brucker [f]

[a] Centre d'Applications et de Recherches en Télédétection, Université de Sherbrooke, Québec, Canada
[b] Centre d'Études Nordiques, Université Laval, Québec, Canada
[c] Landscape Science & Technology, Environment and Climate Change Canada, Ottawa, Ontario, Canada
[d] Climate Research Division, Environment and Climate Change Canada, Toronto, Ontario, Canada
[e] Department of Physical and Environmental Sciences, University of Toronto, Ontario, Canada
[f] NASA Goddard Space Flight Center, Cryospheric Laboratory, Code 615, Greenbelt, MD, USA

ARTICLE INFO

Article history:
Received 12 April 2016
Received in revised form 8 September 2016
Accepted 11 November 2016
Available online xxxx

Keywords:
Rain-on-snow
Ice layers
Snow
Arctic
Passive microwave
Peary caribou

ABSTRACT

Over the past four decades, amplified warming in the Arctic has led to numerous consequences. Of particular relevance, negative anomalies of snow and sea ice cover, glacier retreat, and the extended melt of Greenland combined with increasing temperature at double the rate of the rest of the planet have been observed in the Arctic. Several studies have suggested that another response to the current arctic warming could be an increase in rain-on-snow (ROS) events followed by subsequent freezing and the creation of ice layers. We use recently developed detection algorithms of ROS and ice events using passive microwave retrieval approaches to examine the spatial and temporal trends in rain-on-snow and ice layer creation for 18 islands across the Canadian Arctic Archipelago (CAA) over the last two decades. Results show that both icing and ROS event occurrence tripled between the periods of 1979–1995 and 1996–2011, with very active years in winters 1993–1994, 1998–1999 and 2002–2003. The areas with the most combined occurrences are the Boothia Peninsula and Axel Heiberg, Cornwallis, Banks and Victoria Islands. We then compare the rain-on-snow and icing events to Peary caribou estimates to test whether the algorithms can detect weather events associated with population declines. There has been an important reduction in population numbers of Peary caribou, the northernmost caribou population in Canada, over the last three generations. The major hypothesis for the decline is that severe weather events lead to more difficult winter grazing conditions. The comparison with the Peary caribou population estimates suggest that caribou numbers decrease with increased occurrence of ROS and icing events, where 3–4 ROS events and 1–2 icing events in one winter season are sufficient to have a negative impact on Peary caribou.

Crown Copyright © 2016 Published by Elsevier Inc. All rights reserved.

1. Introduction

Significant climate variability and warming has been observed in the arctic over the past four decades (Serreze et al., 2009; Derksen and Brown, 2012; IPCC, 2014). Over that period, the Arctic has experienced 1.9 times the warming than the rest of the Earth (Winton, 2006; IPCC, 2014), leading to negative trends in snow cover (e.g. Derksen and Brown, 2012) and water equivalent (e.g. Liston and Hiemstra, 2011), sea ice coverage (e.g. Steele et al., 2008; Parkinson, 2014), glacier mass balance (e.g. Papasodoro et al., 2015) and permafrost duration (e.g. Romanovsky et al., 2010). The main reason for the 'Arctic amplification' in global warming is explained by the decreased albedo through the sea ice albedo feedback, but recent studies have shown that this amplification is also caused by the alteration of heat flux exchanges between the ocean and the atmosphere, changes in cloud cover and atmospheric water vapour, soot on snow and atmospheric black carbon (Serreze and Barry, 2011). Given the state of these causative factors, it is expected that the Arctic amplification will become stronger in the near future.

A significant consequence of such warming is the increased occurrence of rain-on-snow (ROS) events (Rennert et al., 2009; Liston and Hiemstra, 2011). Very little is known about ROS in northern regions, and even less about their cumulative impact on the surface energy balance. The water percolation from ROS leads to an accumulation of a significant amount of water at the bottom of the snowpack, which can refreeze (Riseborough et al., 2008; Weismüller et al., 2011. Given the

* Corresponding author at: Centre d'Applications et de Recherches en Télédétection (CARTEL), Département de Géomatique Appliquée, Université de Sherbrooke, Sherbrooke, Québec J1K 2R1, Canada.
E-mail address: a.langlois2@USherbrooke.ca (A. Langlois).

http://dx.doi.org/10.1016/j.rse.2016.11.006
0034-4257/Crown Copyright © 2016 Published by Elsevier Inc. All rights reserved.

current Arctic amplification, ROS events are projected to be more frequent and over a wider spatial extent (Semmens et al., 2013). For instance, Liston and Hiemstra (2011) modeling work suggests an increase in ROS days of +0.03 days/decade and an increase in air temperature of +0.17 °C/decade. However, they did not provide any specific trend for the Canadian Arctic Archipelago (CAA). Furthermore, Putkonen and Roe (2003) modeled a 40% increase in areas impacted by ROS by 2080 by doubling the atmospheric CO_2 levels. Although simulations suggest that ROS and icing events will increase in future, there have been very few studies that have quantified whether there is evidence showing that events have increased at present compared to historical data.

Severe snowpack conditions are hypothesized to decrease forage accessibility or completely prevent foraging by Peary caribou (*Rangifer tarandus pearyi*) (Miller et al., 1982; Aanes et al., 2000; Larter and Nagy, 2001) by creating "locked pastures", a situation where the forage is present but not accessible because it is locked under snow or ice (Vors and Boyce, 2009; Stien et al., 2010). Prolonged and severe weather events have been linked to poor body condition, malnutrition, high adult mortality and calf losses, and major population die-offs in Peary caribou (Parker et al., 1975; Miller and Gunn, 2003). Ouellet et al. (2016) showed that a snow density threshold value can be linked to decreased Peary caribou observations in the Canadian Arctic Archipelago (CAA). This is of particular relevance given that the main cause for reported declines in Peary caribou populations is hypothesized to be linked to snow conditions (COSEWIC, 2004; Johnson et al., 2016). In a similar context, Kohler and Aanes (2004) demonstrated that ROS events explain most of the population variability in growth rate for Svalbard reindeer.

The development of tools such as a satellite approach to monitor ROS and ice layers that would allow for the estimation of the frequency and spatial extent of severe weather events is needed to improve the ability to quantify the magnitude of the effects on Peary caribou populations and consider the potential consequences of future changes in climate on population persistence (Johnson et al., 2016). This was identified as a priority research need for informing Peary caribou management and recovery (Johnson et al., 2016). Given the sensitivity of passive microwave brightness temperatures to wet snow and ice (or snow density), recent studies have attempted to track ROS events and ice layers (e.g. Grenfell and Putkonen, 2008; Rees et al., 2010), but it was concluded that more robust detection algorithms using statistical approaches should be explored. This motivated recent work on the detection of ROS (Dolant et al., 2016) and ice layers (Montpetit et al., 2013) using passive microwave radiometry that now allows the use of satellite remote sensing to track event occurrence since 1979 (a detailed description of both approaches is provided in Section 2.3).

Specifically, we intend to 1) retrieve ROS and ice occurrence for 18 islands of the Canadian Arctic Archipelago for which caribou population counts are available; 2) examine changes in frequency of ROS and ice occurrence across the islands from 1979 to 2011; 3) compare event occurrence with Peary caribou population data; and 4) provide future insight on ROS and ice layer conditions. This worked is centred on two main hypotheses: 1) ROS and icing event occurrence increased since 1979 across the CAA and 2) large caribou numbers are found in years with less occurrence in ROS and icing events. One should not that the ice layers detected by our algorithm can either be from a ROS or a melt event as there are currently no ways to distinguish both types of ice layers.

2. Data and methods

2.1. Study sites

In Canada, caribou are divided into 12 designatable units allowing for a better representation of the species with regards to their habitat (COSEWIC, 2011). Peary caribou are the northernmost designatable unit in Canada. The study area is located in the Canadian Arctic Archipelago (CAA), where Peary caribou are distributed (Johnson et al., 2016). For this study, a total of 18 islands where caribou survey counts are available were analyzed (Fig. 1).

2.2. Passive microwave algorithm details

2.2.1. Rain-on-snow

The rain-on-snow detection approach used in this study was developed by Dolant et al. (2015), where the full details can be found. The algorithm uses passive microwave brightness temperatures (T_B) at 19 and 37 GHz in both horizontal (H) and vertical (V) polarizations, hereinafter referred to as 19H, 19V, 37H and 37V. The method uses the gradient ratio (GR) in both polarizations such that:

$$GR(pol_{(37,19)}) = \frac{[T_B\ (pol,37) - T_B\ (pol,19)]}{[T_B\ (pol,37) + T_B\ (pol,19)]}, \quad (1)$$

Their results have shown that under a ROS event $T_B37H > T_B19H$ and $T_B37V < T_B19V$, which was explained by warmer, wetter and higher emissivity of the snow-air interface at 37H (horizontal polarization being more affected than vertical polarization). They suggested a ratio (GRP) between GR-V and GR-H:

$$GRP = \frac{GR{-}V\ pol}{GR{-}H\ pol}, \quad (2)$$

where a threshold on GRP indicates the presence of ROS (a clear distinction in ROS for GRP < −5 was shown) with lower threshold applied in dense snow (see Results). Since the GRP is calculated using two ratios, noise in the temporal evolution is small, thus no correction is required between the different satellite sensors. Furthermore, it was showed in Dolant et al. (2016) that a melt event was not sufficient to trigger the reversal on which the ROS detection algorithm is based. Furthermore, the amount of water added to the snowpack from a ROS event is far greater, and over a shorter period, which is needed to create the inversion.

2.2.2. Ice detection index

Rain-on-snow events will lead to subsequent ice layer formation, which may be located at the surface, within the snow cover or at the soil/snow interface. Ice layers can be detected using passive microwaves for which an ice detection index (IDI) was developed by Montpetit (2015). The IDI is based on a sensitivity analysis of the Microwave Emission Model of Layered Snowpacks (MEMLS, Wiesmann and Mätzler, 1999) for the effects of the presence of ice lenses within a snowpack. Montpetit et al. (2013) showed that the microwave T_B is very sensitive to the presence of an ice layer and its position within the snowpack due to the very different dielectric contrast between the different layer interfaces (i.e. ice-soil, ice-snow and ice-air) (Fig. 2).

Grenfell and Putkonen (2008) showed that the polarization ratio (PR, Eq. (3)) at 19 and 37 GHz was very sensitive to the presence of ice lenses in the snowpack. This is because the horizontal polarization (H-pol) T_B is more sensitive to layering than the vertical polarization T_B (V-Pol); hence, an increased difference between the T_B in both polarizations results in an increased PR for a given frequency.

$$PR(f) = \frac{T_B(f,V{-}Pol) - T_B(f,H{-}Pol)}{T_B(f,V{-}Pol) + T_B(f,H{-}Pol)} \quad (3)$$

Montpetit (2015) simulated the T_B for 23 measured snowpacks to reproduce realistic snowpack conditions. Next, the simulations were re-run adding ice layers at different positions within the snowpack (at the snow-soil, snow-snow and snow-air interfaces) to examine the effects on the T_B to the presence of ice lenses. Spatial variability was

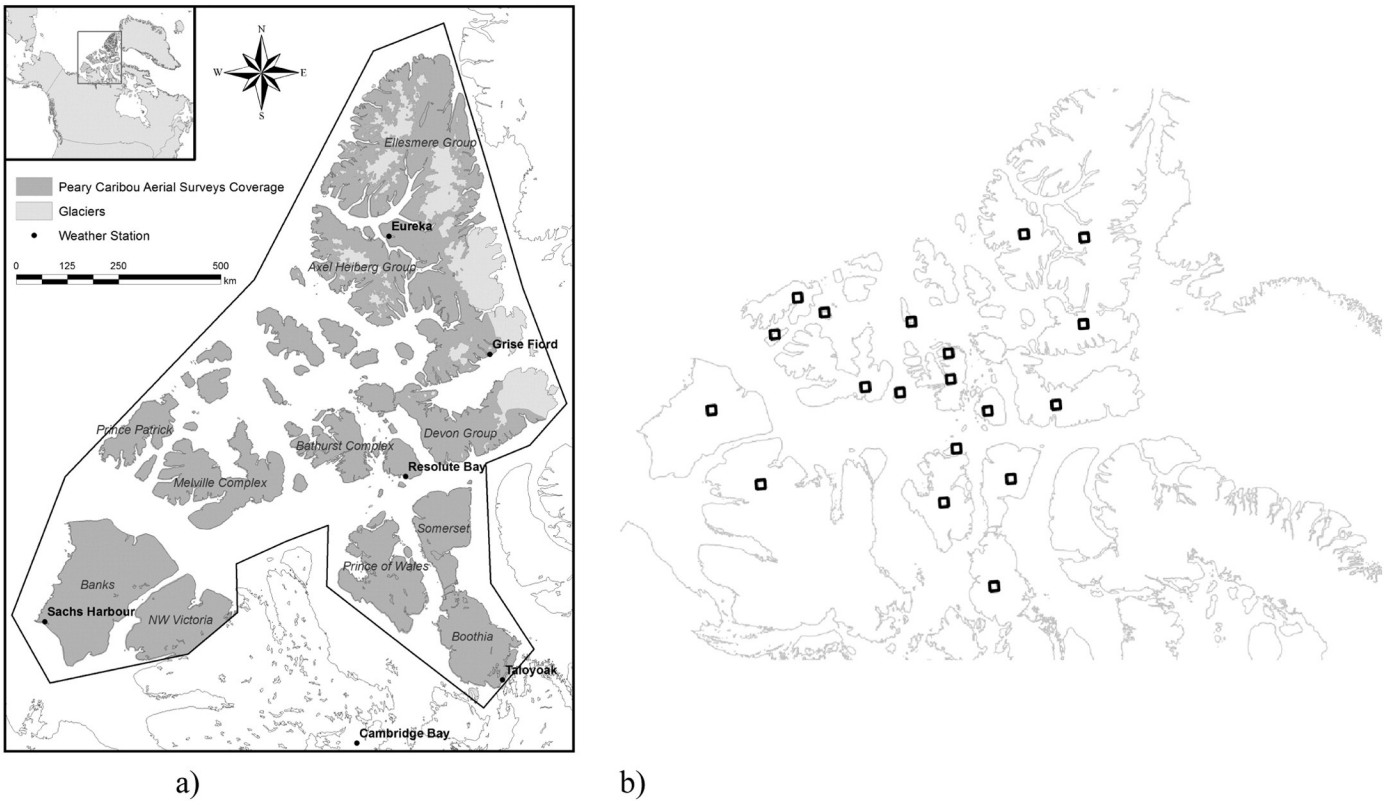

Fig. 1. Study area encompassing the Peary caribou habitat range (a). A total of 18 selected islands/pixels are highlighted, where caribou counts are available between 1979 and 2011 (b).

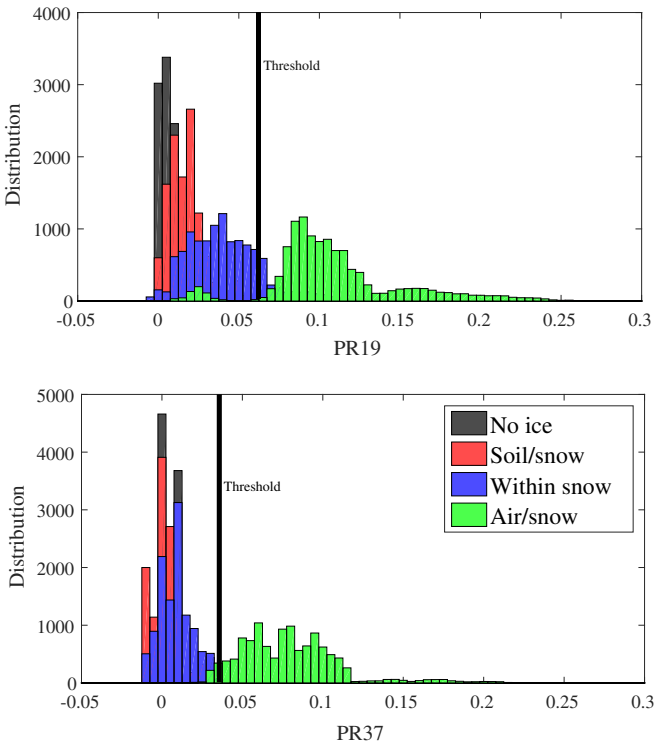

Fig. 2. Histogram distribution of the difference between the simulated PR and the mean PR values of the ice free simulations from Montpetit (2015), 19 (PR19) and 37 GHz (PR37). To normalise the distributions of all four scenarios (ice free, snow surface, within snow and soil/snow interface), the simulations for the ice free scenario were duplicated 20 times to have the same number of points as the other three scenarios.

taken into account by calculating the frequency dependent (f) ΔPR:

$$\Delta PR(f) = PR(f) - \overline{PR}(f) \quad (4)$$

where ($\overline{PR}$) is the winter mean PR at a given frequency f, defined as the winter mean PR value for the snowpack simulations without an ice layer present. Histogram distributions of the simulated ΔPR were produced to identify thresholds between the different snowpack conditions (no ice and ice at the different positions within the snowpack). The easiest conditions to discriminate were the iceless snowpacks from the snowpacks with an ice lens at the surface (snow-air interface) of the snowpack. This is explained by the highest dielectric contrast at the ice-air interface (Montpetit et al., 2013). The histograms were not produced for other types of snow, but it is expected that different thresholds should be used for different snow types/environments (ex. tundra vs maritime).

To properly consider the spatial variability and sensor characteristics of the PR across the 18 islands, an iterative approach to compute the winter mean per pixel and per sensor was used. For a given iteration, the PR mean and standard deviation are calculated for the months of December to March for all the winters of each sensor period. All PR values higher than one standard deviation of the mean of the previous iteration were removed. The mean stabilized and the standard deviation was small after three iterations. The final step is to identify the threshold PR value that allows for the distinction between simulated icing events (see above) and non-icing events.

2.3. Passive microwave satellite data

2.3.1. Frequencies/sensors used

A total of three satellite-borne sensors were used between January 1st, 1979, and December 31st, 2011 to characterize the occurrence of ROS and Icing events across the CAA. Brightness temperatures (T_B) at 19 and 37 GHz were extracted from the Scanning Multichannel

Microwave Radiometer (SMMR) on the Nimbus-7 satellite from January 1st, 1979, to August 20th, 1987 (Knowles et al., 2000). Between August 21st, 1987, and June 18th, 2002, the T_B were extracted from the Special Sensor Microwave Imager (SSM/I), which was flown on the Defense Meteorological Satellite Program (DMSP) satellites (Maslanik and Stroeve, 2004). For the period between June 19th, 2002, and December 31st, 2011, data were extracted from the Advanced Microwave Scanning Radiometer – Earth Observing System (AMSR-E) (Knowles et al., 2006). AMSR-E includes 12 frequencies, of which the two used in this paper are available: 19 and 37 GHz. The daily ascending and descending T_B were extracted T_B on the Equal-Area Scalable Earth Grid (EASE-Grid) for a better and easier match to the North American Regional Reanalysis (NARR) data projection used for atmospheric corrections.

The choice of 19 and 37 GHz was motivated by several factors. First, the use of lower frequency would need first an empirical assessment and we do not have those frequencies on our radiometer suite. Work by Montpetit (2015) showed the potential of detecting ice layers at the bottom of the snowpack, but ran into a much coarser resolution issue. Since some caribou observations were conducted on small islands, it would not be possible to use lower frequencies at those locations. As for snow thickness, across the domain the snow thickness measured at stations during ROS was on average 15.1 cm (7.4 to 24.69 cm), a much smaller value than the penetration depth that can be expected at lower frequencies further motivating the use of 19 and 37 GHz.

2.3.2. Atmospheric corrections using NARR data

Brightness temperatures for all frequencies and sensors were corrected using precipitable water (PWAT) data from the North American Regional Reanalysis (NARR) (Mesinger et al., 2006). NARR data are available at a resolution of 0.3°, which corresponds to a pixel size of approximately 32 km. The PWAT values were extracted over each satellite pixel, and the data are available from 1979 to present, at a 3-hour timestep (8 times daily). The downwelling atmospheric brightness temperature ($T_{B\text{-}atm\downarrow}$) at 19 and 37 GHz were calculated using the relationship between PWAT and T_B from Roy et al. (2012). The Millimeter-wave propagation model (MPM, Liebe, 1989), implemented in the Helsinki University of Technology (HUT: Pulliainen et al., 1999) radiative transfer model was used to compute the relationship between PWAT and $T_{B\text{-}atm\downarrow}$ such that:

$$T_{b-atm\downarrow}(19\ \text{GHz}) = 0.93793 \cdot \text{PWAT} + 8.1502 \qquad R^2 = 0.99; \tag{5}$$

$$T_{b-atm\downarrow}(37\ \text{GHz}) = 0.62651 \cdot \text{PWAT} + 22.569 \qquad R^2 = 0.96; \tag{6}$$

2.4. Peary caribou population

2.4.1. Summer estimates

A time series of Peary caribou estimates are available for 18 islands of the CAA (Table 1). The counts were conducted by aerial surveys between April and July, and have been area corrected to ensure results are comparable in the time series for each island/island group (Johnson et al., 2016). All raw caribou density estimates from aerial surveys were extrapolated to a standardized area (area corrected) to ensure that estimates of total caribou numbers per island or per island group were comparable between years. The area correction involved standardizing for variation in the area surveyed across years and estimating survey coverage in the Canada Albers Equal Area Conic projection. The surveys were conducted periodically with the collaboration of local communities between 1960 and 2013. Since the satellite passive microwave data are available since 1979, the counts used in this study are from 1980 to 2011. For Banks and Victoria islands, the counts are available on average every four years, between 1982 and 2011 (Table 1), which is the most complete dataset available. The number and frequency of surveys for other islands has varied considerably and an infilling model was developed to address gaps in survey data.

Table 1
Island distribution of Peary caribou counts 1980–2011.

Islands	Average area sampled (km^2)	Years surveyed
Banks	70,582	1982; 1985; 1987; 1989; 1991; 1992; 1994; 1998; 2001; 2005; 2010
Minto Inlet/Victoria	17,534	1980; 1987; 1993; 1994; 1998; 2001; 2005; 2010
Boothia Peninsula	32,715	1985; 1995
Prince of Wales	31,686	1980; 1995; 1996; 2004
Somerset	23,818	1980; 1995; 1996; 2004
Axel Heiberg	19,489	1995; 2007
Ellesmere South	25,050	1989; 2005
Ellesmere Central	28,383	1995
Melville	42,220	1987; 1997; 2012
Prince Patrick	15,830	1986; 1997
Eglinton	1550	1986; 1997
Emerald	550	1986; 1997
Byam Martin	1160	1987; 1997
Devon	26,024	2002; 2008
Lougheed	1300	1985; 1997
Bathurst Island Complex	19,266	1985; 1988; 1990–1997; 2001
Cornwallis/L. Cornwallis.	7000/410	1988; 2002; 2013
Helena	220	1985; 1988; 1990–1992; 1995; 1997

2.4.2. Data imputation

2.4.2.1. Data compilation. Peary caribou estimates were calculated using a range of scientific methods, including Jolly's method (Jolly, 1969), Krebs' method (Krebs, 2001) and a distance sampling method (Buckland et al., 2001), for the time series of observations across all islands in the Canadian Arctic Archipelago (CAA). We also used Bayesian imputation to infill missing data in time and space during our study period. One of the fundamental assumptions of our imputation model is that there is a subset of islands that act as the core areas from where the Peary caribou populations migrate, which are defined as “primary islands”. Islands to which Peary caribou migrate are defined as “secondary islands” and/or “satellite islands”. By grouping these islands into complexes, we were able to delineate six geographic clusters across the CAA.

Classification of an island as a primary or secondary/satellite island was based on scientific literature and Aboriginal Traditional Knowledge. In the Banks group, Banks Island was considered as the primary island because historical records suggest that Peary caribou move from Banks Island to northwest Victoria Island (NWV) (Miller, 1986). For the Axel Heiberg cluster, Axel Heiberg Island is the primary island (Jenkins, 2007). For the Melville group, Melville Island is considered the primary island because larger numbers of Peary caribou and higher survival rates are reported on this island compared to the other constituent locations (Miller et al., 1977). In the Bathurst Island Complex, the island with the same name was considered the primary location, because it is the largest island within the complex and supports larger numbers of Peary caribou compared to other satellite islands within the complex that have been surveyed (Jenkins et al., 2011). For the Boothia group, the most frequently surveyed island is Boothia Peninsula. A number of Peary caribou inhabit Boothia Peninsula year round (Johnson et al., 2016).

2.4.2.2. Model description. Our data imputation method is founded on an empirical regression model. The Peary caribou population estimates for secondary islands were predicted from the population of the primary islands, the areal ratio of the pair of islands considered, and the year that we were trying to infill. Bayesian inference was used to estimate model parameters based on the information contained in our dataset.

Thus, the governing equation for predicting population estimates in secondary/satellite islands was as follows:

$$\begin{aligned}\log(mu_{Secondary}) &= \theta_1 + \theta_2 \cdot \log(\delta_i) + \theta_3 \cdot t + \theta_4 \cdot P_{i,t} \cdot \log(PC_{Primary}) \\ &\quad + \theta_5 \cdot (1-P_{i,t}) \cdot \log(PC_{Primary}) \\ \log(PC_{Secondary}) &\sim N(\log(mu_{Secondary}), \sigma^2) \\ \theta_j &\sim MVN(\mu, \textstyle\sum) \quad j = 1, \ldots, 5 \\ \sigma^{-2} &\sim gamma(0.001, 0.001)\end{aligned} \tag{7}$$

where $mu_{Secondary}$ and $PC_{Secondary}$ represent the model prediction and observed population in a secondary or satellite island, respectively; σ^2 represents the associated structural error drawn from an uninformative gamma prior distribution; and $P_{i,t}$ denotes a probabilistic weight, varying from 0 to 1, that characterizes the relative abundance between secondary/satellite and primary islands for location i at year t. Specifically, this weight expresses the likelihood for the population to be higher in the secondary/satellite location relative to the primary one. Our model also explicitly considers the nearly monotonic decline of the Peary caribou population over time by introducing a linear term (in the logarithmic scale): $PC_{Secondary}$ represents the Peary caribou population in secondary/satellite islands; $PC_{Primary}$ represents the population observed in the primary island; δ is the ratio of the area of the secondary/satellite island relative to the primary island area. The parameter vector $\theta = [\theta_1, \theta_2, \theta_3, \theta_4, \theta_5]$ was assumed to follow a multivariate normal distribution, with mean values provided by the vector $\mu = [0,0,0,0,0]$ and the covariance matrix Σ drawn from a Wishart distribution.

After the Bayesian updating, the posterior predictive distribution of the model was used to infill data in secondary/satellite islands using as predictors the observed estimates for primary locations along with the rest of the variables. There were also cases where data gaps existed in primary islands, while the secondary/satellite locations did have population records. In the latter case, we infilled the populations on the primary islands by rearranging the previously described governing equation as follows:

$$\log(mu_{Primary}) = \frac{\log(PC_{second}) - \theta_2 \cdot \log(\delta_i) - \theta_3 \cdot time - \theta_1}{((\theta_4 - \theta_5) \cdot P_{i,t} + \theta_5)} \tag{8}$$

The required parameter samples were drawn from probability distributions, which were generated using Markov Chain Monte Carlo (MCMC) simulations.

Our infilling model has an additional layer that specifies the probabilistic weight, $P_{i,t}$, associated with the relative abundance between secondary/satellite and primary islands for location i at year t. We used a logistic regression model to quantify the likelihood of the secondary/satellite island population being greater than the primary island in a particular year as follows:

$$\begin{aligned}\gamma_{i,t} &\sim \text{Bernoulli}(P_{i,t}) \\ logit(P_{i,t}) &= B_i + b_t \cdot t\end{aligned} \tag{9}$$

where B_i is the spatial cluster-specific intercept and b is the year-specific coefficient connecting the study year t with the probability $P_{i,t}$, $\gamma_{i,t}$ is a binary variable (0 or 1) that indicates the relative Peary caribou abundance between the secondary/satellite and primary location at the specific cluster (i) for a given year (t). For example, if the secondary island has a greater population than the primary one, then γ will be equal to 1; otherwise, γ will be equal to 0.

2.4.2.3. Model computations. We used Bayesian inference to estimate all of the model parameters, while explicitly accommodating the structural and parametric uncertainty (Gelman et al., 2014). Bayesian inference treats each parameter ϑ randomly and, using the likelihood function, it expresses the relative plausibility of obtaining different values of the parameter when particular data have been observed:

$$\pi(\vartheta|data) = \frac{\pi(\vartheta)L(data|\vartheta)}{\int_{\vartheta} \pi(\vartheta)L(data|\vartheta)d\vartheta} \tag{10}$$

where $\pi(\vartheta|data)$ is the posterior probability that expresses our updated beliefs of the parameter, $\pi(\vartheta)$ represents our prior knowledge regarding the probability distribution, and $L(data|\vartheta)$ correspond to the likelihood of observing the data given the different ϑ values. The denominator in Eq. (10) is the expected value of the likelihood function. It acts as a scaling constant that normalises the area under the posterior probability distribution. In this study, we conducted the first Bayesian analysis. Using Markov Chain Monte Carlo (MCMC) simulations (Gilks et al., 1998), we obtained sequences of realizations from the model posterior distributions. For the analysis, we used two chain runs of 50,000 iterations, keeping every 10th iteration (thin of 10) to minimize serial correlation. After the MCMC simulation converged to the true posterior distribution, the samples were taken. The convergence of the sequences occurred after ~5000 iterations (burn-in period).

3. Results

3.1. Temporal analysis 1979–2011

3.1.1. Brightness temperatures

The T_B were extracted for 18 EASE-Grid pixels (centred on surveyed caribou zones) across 18 islands of the Canadian Arctic Archipelago. Table 2 provides the coordinates of each pixel across the 18 islands:

3.1.2. ROS detection

The GRP was calculated for each pixel between 1979 and 2011. The temporal behaviour of the GRP was analyzed according to the thresholds suggested in Dolant et al. (2015). In our study, the GRP values suggest a threshold lower than that reported in Dolant et al. (2015) to avoid noisy satellite signatures, which include heterogeneous contributions so that sharp decreases in GRP were considered as ROS. In Dolant et al. (2015), the GRP reached on average −5 during a ROS, but the mean snow density in their study did not reach 250 $kg \cdot m^{-3}$. In Arctic conditions, the average snow density can easily reach 300–400 $kg \cdot m^{-3}$ because of wind compaction (Derksen et al., 2014), so the GRP threshold should be lower to distinguish ROS in dense snow conditions.

Using ROS observations from three Inuit communities in Nunavik, Québec, Canada (Salluit, Kangiqsujuaq and Kangirsuk), we extracted

Table 2
EASE-Grid and geographic coordinates for the 18 pixels.

			EASE-Grid coordinates		Geographic coordinates	
Islands	Pixel ID	% land	X	Y	Lat. (N)	Long. (W)
Boothia Peninsula	BP1	100	275	354	70,533	−94,5
Prince of Wales	PW1	100	285	349	72,617	−99
Somerset	SI1	100	288	357	73,35	−93.25
Axel Heiberg	AH1	100	316	361	79,817	−89,683
South Ellesmere	SE1	100	304	368	77,067	−83,283
Central Ellesmere	1CE	100	314	368	79,333	−81,467
Melville	MI1	100	299	341	75,367	−107,667
Prince Patrick	PPI1	100	310	334	76,9	−118,017
Eglinton	EgI1	68	306	331	75,783	−118,417
Emerald	EmI1	54	308	337	76,8	−114,1
Byam Martin	BMI1	89	298	345	75,217	−104,217
Devon	DI1	100	295	363	75,017	−88,333
Lougheed	LI1	41	307	347	77,3	−104,933
Cornwallis	CI1	100	295	355	75,133	−95,1
Helena	HI1	85	302	351	76,5	−99,883
Bathurst Is. Com.	BIC1	100	299	351	75,783	−98,867
Banks	BI1	100	302	322	74,005	−123,465
Victoria (Minto)	VI1	100	292	327	72,593	−116,232

GRP values for 39 ROS events for winter 2010–2011 for the three stations (see Dolant et al., 2015). The average GRP for observed ROS was −5, with minimum values of −45, −80 and −40 for Salluit, Kangiqsujuaq and Kangirsuk, respectively, suggesting a lower threshold in arctic conditions. We further looked at the events where only rain was observed (no mixed precipitation, fog, etc.) and the average GRP decreased to −10, which is the threshold used in this paper. Fig. 3 highlights the temporal evolution of GRP for Prince of Wales and Banks islands and occurrences for all islands are provided in Table 3.

In Table 3, one can clearly see an increase in ROS events between the periods 79–80/94–95 compared to the period 95–96/10–11. The cumulative observed ROS in the first period is 102 (26% of all observed ROS) and 284 (74% of all observed ROS) in the latter. This suggests a significant increase in ROS occurrence, with the most active years being 02–03, 08–09, 98–99 and 93–94. Of particular relevance, we can see that AH, BMI, CI and PW are the islands with the highest ROS occurrence since 1979. A more detailed discussion on comparing ROS and IDI is provided in Section 3.1.4.

3.1.3. IDI detection

As mentioned earlier, the mean polarization ratio (PR) was calculated on a sensor/pixel basis to avoid bias linked to a different sensor when targeting ice crusts. The mean winter PR was calculated between December 1st and March 31st and averaged over each satellite period (i.e. SMMR, SSM/I and AMSR-E) and values for each pixel are shown in Table 4.

As mentioned in the previous section, from PR and mean winter PR values, the ΔPR can be calculated for which a threshold can be applied for ice detection. Modeling work from Montpetit (2015) suggested distributions of ΔPR values for various ice crust vertical location scenarios from which thresholds were established. For our study, the thresholds are 0.060 for ΔPR 19 GHz and 0.035 for ΔPR 37 GHz (see Montpetit, 2015). From the mean winter PR values above, the ΔPR was calculated for which the thresholds in Fig. 2 can be applied and Fig. 4 depicts an example of ΔPR for 19 and 37 GHz.

In Fig. 4, it becomes possible to identify ice layer events throughout the study period. One event that was discussed in the literature is the ROS and icing that occurred over Banks Island in October 2003 (Grenfell and Putkonen, 2008). This event is clearly seen using the ΔPR as shown in Fig. 5 in the shaded box centred on October 2003:

We thus applied the thresholds to the 18 islands for the 1979–2011 period and Table 5 summarizes the detected ice layers.

The data show an increase in icing events between the periods 1979–1995 and 1995–2011 (Table 5). Over the 32-year observation period across the 18 pixels, a total of 222 events were detected using the polarization ratio approach. Of the 224 events, 56 (25%) were observed between 1979 and 1995, while 166 (75%) were observed between 1995 and 2011. This increase in occurrence is the same as the increase in ROS events (Table 3). Of particular relevance, the most active years were 1988–1989, 1993–1994, 1998–1999, 2002–2004, and 2007–2009. A discussion on the climatological context is provided in the next section. As for the pixels/islands chosen, it appears that 7 (BP, AH, BM, DI, CI, BI and VI) of the 18 islands accumulated 19+ ice events with a maximum of 32 events observed for Boothia Peninsula.

3.1.4. Discussion of ROS and IDI trends

Interestingly, both ROS and IDI, that are based on different T_B approaches, suggest an overall increase in occurrence of ice layer formation within the snowpack across the study area between 79 and 90/94–95 and 95–96/1011. A ROS event will not automatically lead to an ice layer or, at least, one of significant thickness to be detected using the ΔPR approach. This is why the numbers for ROS occurrence are greater compared with IDI in general. When we compare both types of events on a yearly basis, the most active years are 88–89, 93–94, 98–99, 02–03, 03–04, 07–08 and 08–09 (in no particular order, see Fig. 6a). In terms of locations, Fig. 6b suggests that the most 'active' areas are, in order, Boothia Peninsula, Byam Martin, Banks and Victoria Islands.

Similarly, Ouellet et al. (2015) reported that Boothia Peninsula may be more prone to warming and dense snow conditions in the near future, potentially leading to unfavourable grazing conditions for Peary caribou. This suggests some congruence in the detection of icing events based on passive microwave radiometry (herein) and simulations using snow models (Ouellet et al. 2015).

Despite of all, some uncertainties remain. The very high number of ROS events observed in 2002–2003 is mostly related to Axel Heiberg Island, where a total of 46 events were recorded in that particular winter. When looking at the temporal evolution of GRP, we do see an increase in variability throughout the season with peaks reaching the threshold set at −10. We investigated the source of variability (NARR, uncorrected brightness temperatures) and it turned out to be a sensor issue. When we focus on the 2002–2003 season, we can clearly see periodic peaks, both negative and positive that cannot be accounted for ROS since they reach the threshold. However, it is hard to conclude on how many of the 46 'detected' events are from the sensor issue, and how

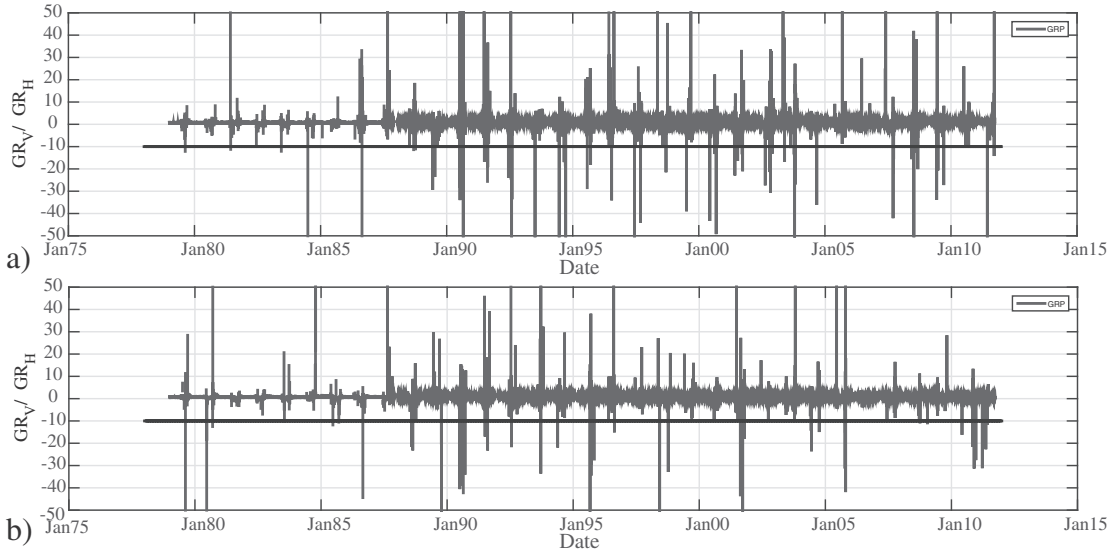

Fig. 3. Evolution of GRP values between 1979 and 2011 for a) Prince of Wales and b) Banks islands. The detection threshold is set at −10.

Table 3
Number of rain-on-snow (ROS) events analyzed from October 1st to May 31st of each winter season using a GRP threshold of −10.

	79–80	80–81	81–82	82–83	83–84	84–85	85–86	86–87	87–88	88–89	89–90	90–91	91–92	92–93	93–94	94–95	Totals 79–95
BP1	0	0	**1**	0	0	0	**1**	0	**1**	0	0	0	0	0	**2**	0	**5**
PW1	0	0	0	0	0	0	**1**	0	0	**1**	**2**	0	0	0	**1**	0	**5**
SI1	**1**	0	**1**	0	0	0	**1**	**1**	0	0	0	0	0	0	**2**	0	**6**
AH1	0	0	0	0	0	0	**1**	0	0	0	0	0	0	0	0	0	**1**
SE1	0	0	0	0	0	0	**2**	**1**	0	0	**4**	0	0	0	0	0	**7**
CE1	0	0	**1**	**2**	0	0	**2**	0	0	**1**	0	0	0	0	**4**	0	**10**
MI1	0	0	0	**1**	0	0	**1**	0	0	0	0	0	0	0	**1**	0	**3**
PPI1	0	0	0	0	0	0	0	0	0	**1**	0	0	0	0	0	0	**1**
EgI1	0	**1**	0	0	0	0	0	0	0	**1**	0	0	0	0	0	0	**1**
EmI1	0	0	0	0	0	0	0	0	0	**2**	0	0	0	0	0	**2**	**4**
BMI1	0	0	0	0	**1**	0	0	0	0	**6**	**2**	**3**	0	**1**	**7**	**2**	**22**
DI1	0	**1**	0	0	0	0	**1**	**1**	0	**1**	0	0	0	**1**	**3**	0	**8**
LI1	0	0	0	0	0	**1**	0	0	0	0	0	0	0	0	**2**	0	**3**
CI1	0	0	**2**	**1**	0	0	**2**	0	0	**1**	0	**3**	0	0	**3**	0	**12**
HI1	0	0	**1**	0	0	**1**	**1**	**1**	0	0	0	0	**1**	0	**1**	0	**6**
BIC1	0	0	0	0	0	0	**1**	0	0	0	0	0	0	0	0	0	**1**
BI1	0	0	**1**	0	0	0	0	0	**1**	0	0	0	0	0	**2**	0	**4**
VI1	0	0	0	0	0	**1**	0	**1**	0	0	0	0	0	0	**1**	0	**3**
Totals	1	2	7	4	1	3	14	5	2	14	8	6	1	2	29	4	102

	95–96	96–97	97–98	98–99	99–00	00–01	01–02	02–03	03–04	04–05	05–06	06–07	07–08	08–09	09–10	10–11	Totals 95–11	1979–2011
BP1	0	0	0	**3**	**1**	0	0	0	0	**2**	**2**	**1**	0	**2**	0	0	**11**	**16**
PW1	**1**	0	0	**1**	0	0	**1**	0	**1**	**2**	**5**	0	**1**	**4**	0	**5**	**21**	**26**
SI1	0	0	**1**	0	0	0	0	0	0	0	**3**	0	**1**	**4**	0	0	**9**	**15**
AH1	**1**	0	**1**	**1**	0	0	0	**46**	**2**	**8**	**2**	**1**	0	0	0	0	**62**	**63**
SE1	**1**	0	**1**	**1**	0	0	0	**1**	0	0	0	0	0	0	0	0	**4**	**11**
1CE	0	**1**	0	1	0	0	0	0	0	0	0	0	0	0	0	0	**2**	**12**
MI1	0	0	0	0	0	0	0	0	0	**1**	0	0	0	**2**	**1**	0	**4**	**7**
PPI1	0	0	**1**	0	0	0	0	**6**	**2**	**1**	0	0	0	0	0	**2**	**12**	**13**
EgI1	0	0	0	0	0	0	0	0	0	0	**3**	**4**	**3**	**4**	**3**	0	**17**	**18**
EmI1	**2**	0	0	0	0	0	0	**13**	0	0	**2**	**2**	0	**3**	0	**2**	**24**	**28**
BMI1	**4**	**2**	**2**	**14**	**3**	**1**	**7**	**2**	0	**2**	0	**3**	0	**1**	0	0	**41**	**63**
DI1	0	**3**	**1**	**1**	0	0	0	0	0	0	**1**	**2**	**2**	**2**	0	0	**12**	**20**
LI1	0	0	0	**3**	0	0	0	**2**	**1**	0	0	**1**	0	**3**	0	0	**10**	**13**
CI1	0	**1**	0	**1**	**1**	**1**	**1**	0	**1**	**1**	**1**	**1**	**1**	**11**	0	**1**	**22**	**34**
HI1	0	0	0	0	0	0	0	**1**	**1**	0	0	**1**	0	**1**	0	0	**4**	**10**
BIC1	0	**2**	0	0	0	0	0	**1**	0	0	**1**	**2**	0	**1**	0	0	**7**	**8**
BI1	0	0	0	**3**	**1**	0	0	**2**	**1**	0	0	0	0	**2**	0	0	**13**	**17**
VI1	0	0	0	0	0	0	0	0	**4**	0	**1**	0	0	**2**	**2**	0	**9**	**12**
Totals	9	9	7	29	6	2	9	74	13	17	21	18	8	42	10	10	284	386

many are real. If we consider this in the occurrence statistics, 30% of the total occurrence was observed between 1979 and 1995 while 70% occurred between 1995 and 2011, also suggesting an acceleration in ROS occurrence. One should note that this sensor issue was not observed for other 'active' years.

Table 4
Mean winter PR values for each island and sensor.

Pixel ID	Mean PR SMMR		Mean PR SSM/I		Mean PR AMSR-E	
	19 GHz	37 GHz	19 GHz	37 GHz	19 GHz	37 GHz
BP1	0.0516	0.0614	0.0467	0.0453	0.0575	0.0559
PW1	0.0539	0.0663	0.0482	0.0468	0.0605	0.0580
SI1	0.0575	0.0709	0.0485	0.0482	0.0626	0.0638
AH1	0.0540	0.0647	0.0475	0.0467	0.0584	0.0547
SE1	0.0491	0.0556	0.0448	0.0432	0.0381	0.0392
CE1	0.0577	0.0580	0.0488	0.0495	0.0303	0.0311
MI1	0.0515	0.0632	0.0484	0.0493	0.0553	0.0572
PPI1	0.0503	0.0631	0.0469	0.0468	0.0541	0.0562
EgI1	0.0450	0.0536	0.0448	0.0441	0.0458	0.0443
EmI1	0.0483	0.0595	0.0453	0.0397	0.0475	0.0462
BMI1	0.0421	0.0491	0.0445	0.0385	0.0508	0.0476
DI1	0.0527	0.0633	0.0481	0.0441	0.0541	0.0525
LI1	0.0458	0.0543	0.0455	0.0398	0.0481	0.0449
CI1	0.0522	0.0636	0.0518	0.0476	0.0576	0.0567
HI1	0.0494	0.0598	0.0480	0.0447	0.0503	0.0491
BIC1	0.0519	0.0644	0.0541	0.0510	0.0591	0.0583
BI1	0.0476	0.0594	0.0467	0.0453	0.0495	0.0502
VI1	0.0496	0.0647	0.0503	0.0493	0.0527	0.0541

Another source of potential error in the occurrence is the presence of water in the satellite pixel. On Table 2, the fraction of land within the pixel was provided, and one can observe that 6 pixels have partial ocean coverage. The choice of pixel was driven by caribou observations, and so that compromises of ocean presence had to be made. However, of the 6 pixels 3 have a land % higher than 73% so that the effect of ocean for these pixels can be ignored. The pixels with most ocean coverage are: Emerald Island, Eglinton Island and Lougheed Island with coverage of 46, 32 and 59% respectively. The coastal effect of sea ice depends on roughness that increases scattering and decrease the polarization effect (Langlois et al., 2008). Although an increase in scattering could lead to detection commission by our algorithm, a decrease of the polarization effect would have the opposite behaviour. It was suggested in Tables 3 and 5 that considering all 18 pixels, the occurrence of both ROS and IDI tripled between the periods 1979–1995 compared to 1995–2011. A safer assessment of tboth ROS and IDI occurrences would be to remove the islands of Axel Heiberg (sensor issue mentioned above), Emerald, Eglinton and Lougheed. By doing so, the occurrence of ROS events for 1979–1995 is 93 (29%), compared to 229 (71%) events for 1995–2011. For the IDI, the occurrence for 1979–1995 is 54 (36%), compared to 95 (64%) events for 1995–2011 so that the conclusion on an acceleration of event occurrence remains the same, at similar proportions.

As for the differences between sensors, it was stated earlier that the ΔPR are calculated individually for each island, each winter and the detection is based on a 'departure from average' basis. Consequently, the IDI is not influence by differences in sensors. As for the GRP, the only

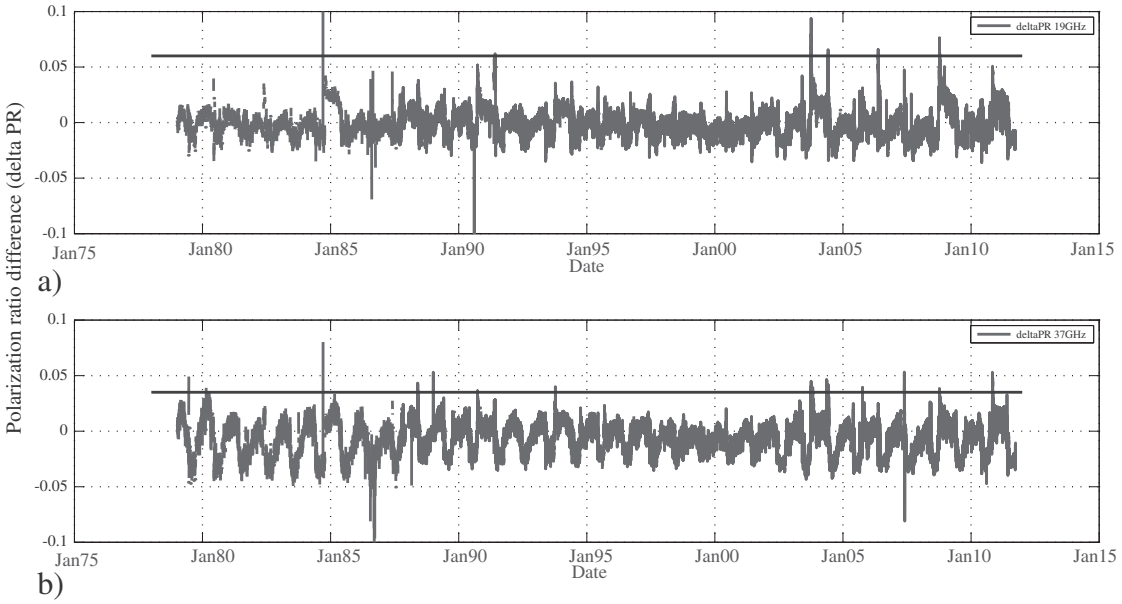

Fig. 4. Temporal evolution of the ΔPR at a) 19 and b) 37 GHz with the ice detection threshold set respectively at 0.06 and 0.035 for a pixel over Victoria Island, Nunavut.

difference seen is the smaller noise in the GRP (depicted in Fig. 3) in SMMR owing to a single daily pass. Using a ratio of ratio (GR_V/GR_H) significantly reduces noise and average GRP values from one sensor to another cannot explain the trend observed in Table 3. For instance, the average GRP values for Victoria Island are 0.67, 0.62 and 0.9 for SMMR, SSM/I and AMSR-E respectively. This level of variability will not influence a detection threshold which is set conservatively at −10 (see discussion on threshold in Section 3.1.2). Furthermore, we extracted GRP, deltaPR19 and deltaPR37 values from one pixel on Banks Island (winter 2004–2005). Values were extracted from SSMI and AMSR-E to further confirm the fact that the developed approaches are not affected by differences in sensors. The results are not shown here, but demonstrate that both sensors are seeing the exact same occurrence of events and that residuals on GRP and deltaPR values are not important enough to cause omissions and/or commissions based on the thresholds used.

Finally, other sources of uncertainties could potentially arise from atmospheric effects and changing snow stratigraphy. From the results presented in Dolant et al., the approach works for arctic snow which is typically composed of two main layers, i.e. hard snow drifts on top of an important hoar layer. The presence of ice layers and water at the surface are more important than the scattering effect from the snow grains (Montpetit, 2015), and thus would not affect the retrieval. As for the atmospheric corrections, the cold cloud temperatures cannot lead to the reversal (commissions). As for potential omissions, a cloud would

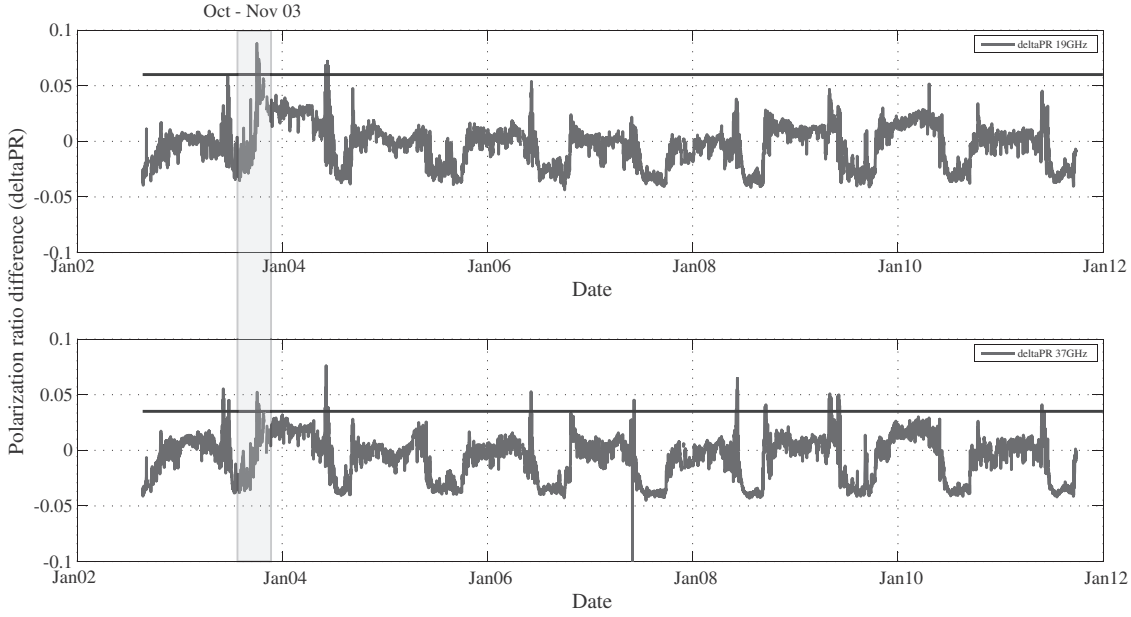

Fig. 5. ΔPR at a) 19 and b) 37 GHz during the AMSR-E period including the period where significant ROS and ice layers were reported in the literature over Banks Island (Grenfell and Putkonen, 2008).

Table 5
Number of ice layer events within snow. The events are analyzed from October 1st to May 31st of each winter season using the ΔPR thresholds of 0.060 and 0.035 for 19 and 37 GHz respectively.

	79–80	80–81	81–82	82–83	83–84	84–85	85–86	86–87	87–88	88–89	89–90	90–91	91–92	92–93	93–94	94–95	Totals 79–95
BP1	0	0	0	0	0	0	0	0	0	**1**	0	0	0	0	**12**	0	**13**
PW1	0	0	0	0	0	0	0	0	0	**1**	0	0	0	0	**3**	0	**4**
SI1	0	0	0	0	0	0	0	0	0	**2**	0	0	0	0	**3**	0	**5**
AH1	0	0	0	0	0	0	0	0	0	**2**	0	0	0	0	0	0	**2**
SE1	0	0	0	0	0	0	0	0	0	0	0	0	0	0	**2**	0	**2**
CE1	0	0	0	0	0	0	0	0	0	**3**	0	0	0	0	0	0	**3**
MI1	0	0	0	0	0	0	0	0	0	**5**	0	0	0	0	0	0	**5**
PPI1	0	0	0	0	0	0	0	0	0	**4**	0	0	0	0	0	0	**4**
EgI1	0	0	0	0	0	0	0	0	0	0	0	0	0	0	0	0	**0**
EmI1	0	0	0	0	0	0	0	0	0	0	0	0	0	0	0	0	**0**
BMI1	0	0	0	0	0	**1**	0	0	0	0	**1**	0	0	0	0	0	**2**
DI1	0	0	0	0	0	0	0	0	0	0	0	0	0	0	0	0	**0**
LI1	0	0	0	0	0	0	0	0	0	0	0	0	0	0	0	0	**0**
CI1	0	0	0	0	0	0	0	0	0	0	0	**1**	**1**	0	**1**	0	**3**
HI1	0	0	0	0	0	0	0	0	0	0	0	0	0	0	0	0	**0**
BIC1	0	0	0	0	0	0	0	0	0	0	0	0	0	0	0	0	**0**
BI1	0	0	0	0	0	0	0	0	0	**1**	0	0	0	0	**12**	0	**13**
VI1	0	0	0	0	0	0	0	0	0	0	0	0	0	0	0	0	**0**
Totals	0	0	0	0	0	1	0	0	0	19	1	1	1	0	33	0	56

	95–96	96–97	97–98	98–99	99–00	00–01	01–02	02–03	03–04	04–05	05–06	06–07	07–08	08–09	09–10	10–11	Totals 95–11	1979–2011
BP1	0	0	**2**	**2**	0	0	0	0	0	0	0	0	**15**	0	0	0	**19**	**32**
PW1	0	0	0	0	0	0	0	0	0	0	0	0	0	0	0	0	**0**	**4**
SI1	0	0	**1**	0	0	0	0	0	0	0	0	0	0	0	0	0	**1**	**6**
AH1	0	0	0	0	0	0	0	**10**	0	**7**	0	0	0	0	0	0	**17**	**19**
SE1	0	0	0	0	0	0	0	0	0	0	0	0	0	0	0	0	**0**	**2**
CE1	0	0	0	0	0	0	0	0	0	0	0	0	0	0	0	0	**0**	**3**
MI1	0	0	0	0	0	0	0	0	0	0	0	0	0	0	0	0	**0**	**5**
PPI1	0	0	0	0	0	0	0	0	0	0	0	0	0	0	0	0	**0**	**4**
EgI1	0	0	0	0	0	0	0	**1**	**1**	0	0	0	0	**3**	0	0	**5**	**5**
EmI1	0	0	0	**3**	0	0	0	0	0	0	0	0	0	**3**	0	0	**6**	**6**
BMI1	**1**	**3**	0	**20**	0	**1**	**3**	0	0	0	0	0	0	0	0	0	**28**	**30**
DI1	0	**1**	0	0	0	0	0	0	**1**	0	0	0	0	0	0	0	**2**	**2**
LI1	0	0	0	**13**	0	0	0	0	0	0	0	0	0	**4**	0	**3**	**20**	**20**
CI1	0	**2**	0	**4**	**5**	0	**3**	0	0	0	0	0	0	**5**	0	0	**19**	**22**
HI1	0	0	0	**6**	0	0	**1**	0	0	0	0	0	0	0	0	0	**7**	**7**
BIC1	0	0	0	**1**	0	0	0	0	0	0	0	0	0	0	0	0	**1**	**1**
BI1	0	0	**2**	**2**	0	0	0	0	**7**	0	0	0	0	**3**	0	0	**14**	**27**
VI1	0	0	0	0	0	0	0	0	**8**	0	**2**	**6**	0	**10**	0	**1**	**27**	**27**
Totals	1	6	5	51	5	1	7	11	17	7	2	6	15	28	0	4	166	222

need to strongly scatter the increase in 37 GHz created from the reversal. From the Dolant surface-based radiometer measurements (i.e. no atmospheric effects), the increase in 37 GHz during the reversal oscillated around 30–40 K. When looking at the atmospheric correction impacts in our study, the impact of atmosphere at 37 GHz varied between 4 and 14 K so that no omissions either can be triggered by the atmosphere.

3.2. Correlation with caribou population numbers

Results for ROS and IDI occurrences were compared to Peary caribou estimates to evaluate the impact of ice layers on grazing conditions. First, ROS occurrence numbers from Table 3 were compared with matching island estimates (Fig. 7a). Winters with more than three ROS events are associated with lower summer caribou numbers, whereas winters with rare-to-no ROS events are associated with higher caribou numbers. ROS events can be punctual in nature, both in time and space, but we expected the decrease in caribou numbers to be more pronounced following numerous ROS events. In Fig. 7b, we compared the same caribou numbers with the presence of ice layers (Table 5) detected using the threshold on ΔPR. The results are consistent with the hypothesis that ice hinders grazing conditions for Peary caribou, suggesting that Peary caribou numbers are lower when 1 to 2 winter events are detected.

3.3. Future outcomes and discussion

Our results suggest the islands with the most substantial increase in ROS are Axel Heiberg (+61 events between 79 and 95 compared to 95–11), Emerald (+21), Byam Martin (+19), Eglinton and Prince of Wales (both at +16) over the 16-years examined. Only 3 islands had fewer occurrences in the second period: Central Ellesmere (−8), Southern Ellesmere (−3) and Helena Island (−2). For IDI, the most important increase in occurrence was observed for Victoria (+27), Byam Martin (+26), Lougheed (+20), Cornwallis (+16) and Axel Heiberg (+15). Interestingly, six islands had a lower occurrence of IDI and most are located in the northern part of the CAA, in agreement with the ROS results.

There is a fair amount of variation in the relationship between Peary caribou numbers and the occurrence of ROS and IDI, especially in the absence of events where Peary caribou numbers range from very low values to >10,000 animals. However from a behavioural perspective, we did not expect to have a statistical trend with population with regard to either ROS or IDI but rather expect a sharp transition when the 'tolerance' to difficult winter grazing conditions is met. Furthermore, Peary caribou populations are affected by a number of factors other than ROS and IDI. For instance, sea ice coverage will have an impact on migratory patterns (Miller et al., 2005), which can affect numbers on a given island for any occurrence of ROS or IDI (see Johnson et al., 2016 for more detailed discussion on threats to Peary caribou). Another factor limiting

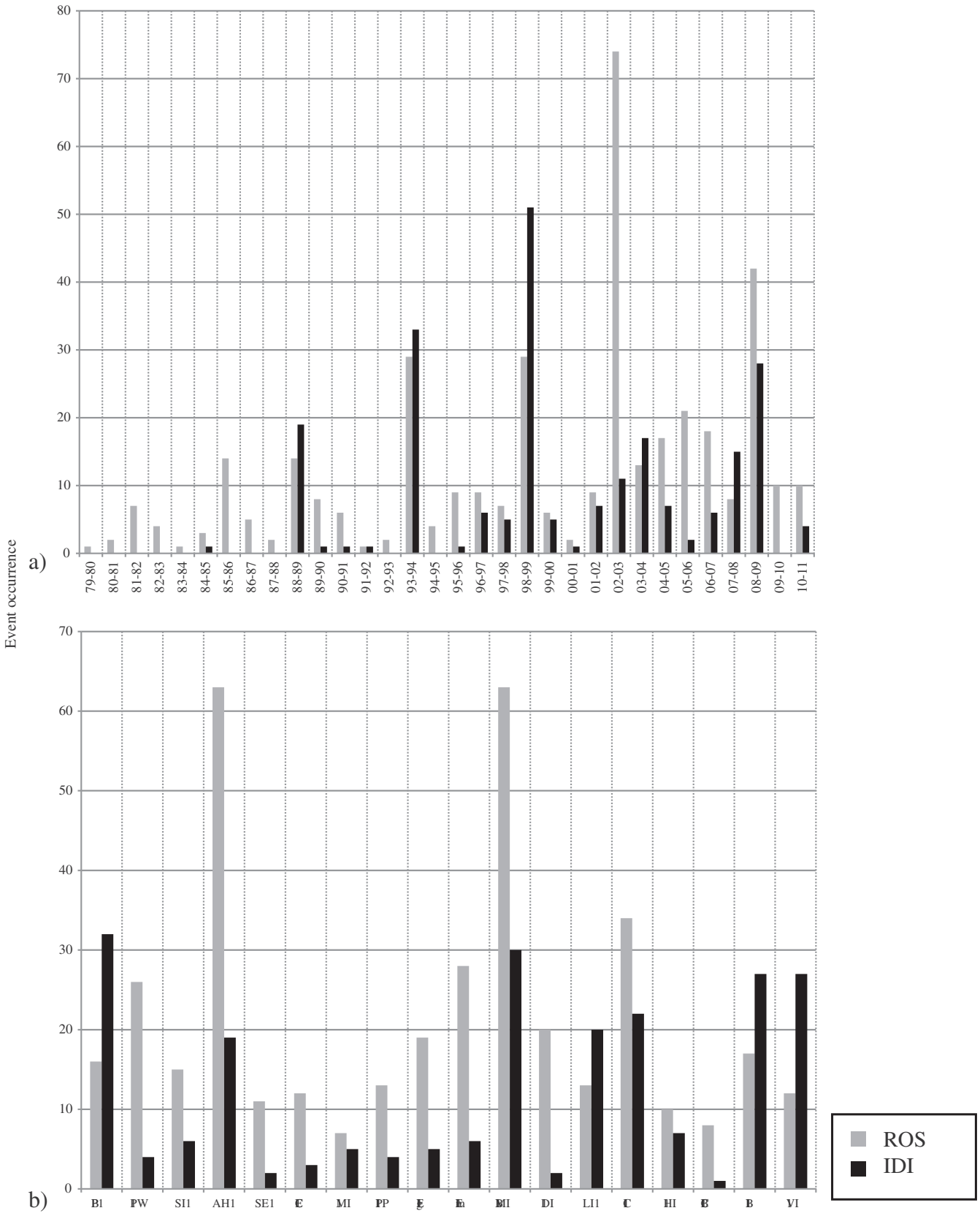

Fig. 6. a) ROS and IDI temporal evolution combined for the 18 islands between 1979 and 2011 and b) ROS and IDI occurrence for each individual island.

the analysis is the availability of Peary caribou abundance estimates. The infilling approach allowed us to maximize data for years where partial surveys were conducted (i.e. only certain island were surveyed). Finally, the T_B were extracted locally over one pixel (25×25 km) per island. The data did not suggest great variability in T_B within one island, but current work in our group is looking at running the algorithms on all CAA pixels.

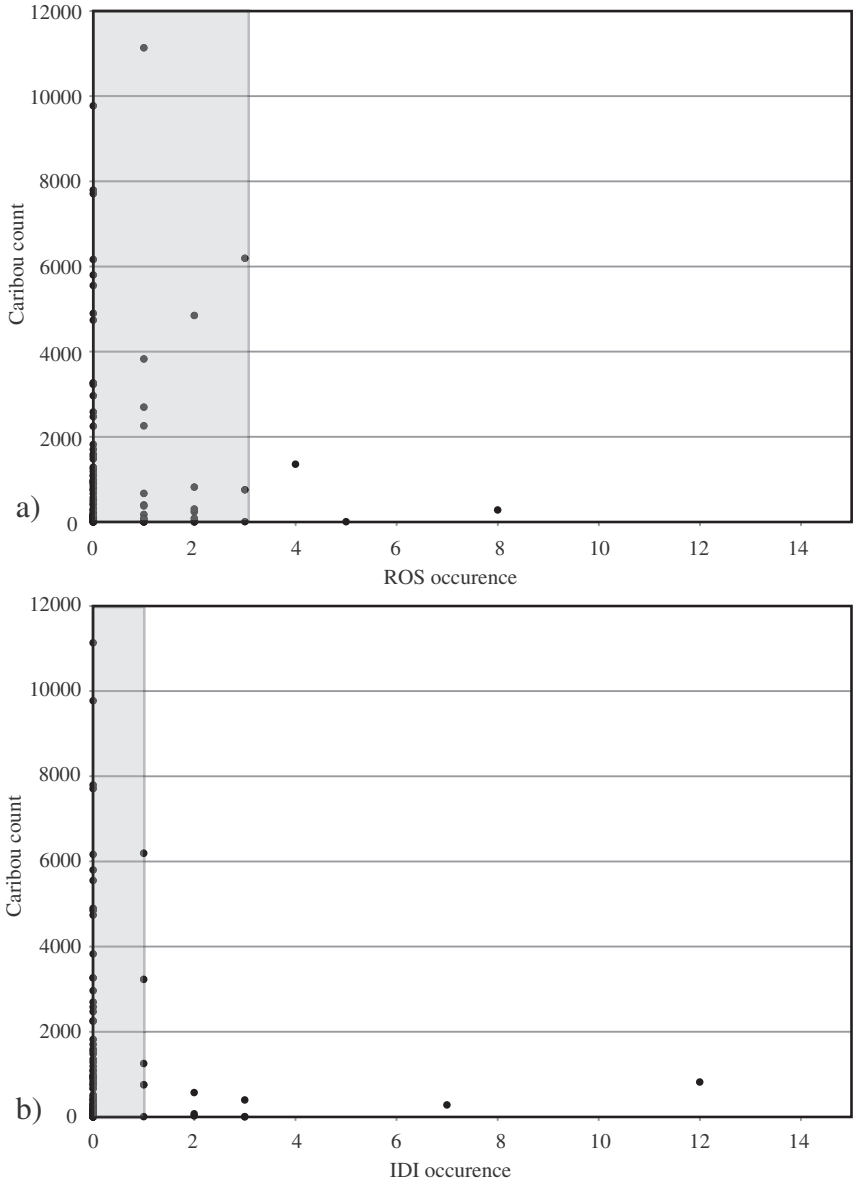

Fig. 7. Comparison between Peary caribou counts and a) ROS, and b) IDI occurrence during the winter season prior to the summer count. The shaded areas highlights high caribou population.

Numerous observations of ROS and IDI using our two passive microwave approaches could not be matched to Peary caribou estimates due to the lack of aerial surveys. Despite the potential limitations, the results presented in Fig. 7, do suggest a negative impact of ROS and IDI occurrence on Peary caribou populations, where higher Peary caribou estimates are associated with lower occurrences of ROS and IDI. Moreover, there is much less variability (<1000) in the low Peary caribou estimates corresponding to years where IDI events are detected. This makes sense given the fact that not all ROS events will lead to an ice layer of sufficient thickness to have a negative impact on grazing conditions.

4. Conclusions

This paper aimed to quantify rain-on-snow and icing events in the Canadian Arctic Archipelago for islands where caribou counts are available. It was shown that for both ROS and IDI, a similar acceleration in event occurrences was observed when comparing 1979–1994 to 1995–2011 with about 75% of the events occurring in the latter period. Our analyses also suggest that the regions located in the southern part of the CAA are more prone to increasing event occurrence. More work is required to better understand linkages to surface temperature anomalies, atmospheric circulation (i.e. precipitation phase transitions, boundary layer mixing) and event occurrence, while targeting sensor problems as highlighted earlier. Ultimately, daily maps of event occurrence will be produced using the approach, which will be meaningful to numerous studies such as caribou survival assessment.

Possible correlations with observed caribou population estimates were investigated to provide future insight with regard to trend occurrence and Peary caribou survival. The next intuitive step will look at critical periods of the Peary caribou life cycle: summer foraging and fall breeding (July – October), winter foraging (November–March) and spring calving (April–June). Statistical relationships between event occurrences per period will be established.

Having an increase in ROS and IDI occurrences can be expected given the increasing air temperature in the Arctic since the early 1980s (Jones et al., 2012). Furthermore, Serreze and Barry (2011) showed that the Arctic amplification has accelerated the rate of warming since 2000

with winter and spring showing the most important trends at 1.73 and 1.59 °C /100 years respectively, which is particularly relevant from a ROS and IDI perspective. With the associated increased cloudiness with sea ice vanishing (Liu et al., 2012); it is likely that the increasing trend in ROS and IDI will continue. Thus, with a sustained arctic warming amplification, along with the increased occurrence of winter storms, it is anticipated that ROS and icing events that affect winter foraging conditions for Peary caribou will continue to increase in the near future. There is a clear need to establish protocols to monitor ROS and ice layers to evaluate winter forage conditions for Peary caribou under a long-term conservation strategy that considers a range of threats to population condition.

References

Aanes, R., Sæther, B.E., Oritsland, N.A., 2000. Fluctuations of an introduced population of Svalbard reindeer: the effects of density dependence and climatic variation. Ecography 23, 437–443.

Buckland, A.T., Burnham, K.P., Laake, J.L., Borchers, D.L., Thomas, L., 2001. Introduction to Distance Sampling: Estimating Abundance of Biological Populations. Oxford University Press, New York.

Climate Change, 2014. In: Core Writing Team, Pachauri, R.K., Meyer, L.A. (Eds.), Synthesis Report. Contribution of Working Groups I, II and III to the Fifth Assessment Report of the Intergovernmental Panel on Climate Change. IPCC, Geneva, Switzerland (151 pp).

COSEWIC, 2004. Assessment and Update Status Report on the Peary Caribou *Rangifer tarandus pearyi* and the Barren-ground Caribou *Rangifer tarandus groenlandicus* (Dolphin and Union Population) in Canada. Committee on the Status of Endangered Wildlife in Canada, Ottawa, Ontario, Canada.

COSEWIC, 2011. Designatable Units for Caribou (*Rangifer tarandus*) in Canada. Committee on the Status of Endangered Wildlife in Canada, Ottawa, Ontario, Canada.

Derksen, C., Brown, R., 2012. Spring snow cover extent reductions in the 2008–2012 period exceeding climate model projections. Geophys. Res. Lett. 39 (L19504), 1–6.

Derksen, C., Lemmetyinen, J., Toose, P., Silis, A., Pulliainen, J., Sturm, M., 2014. Physical properties of Arctic versus subarctic snow: implications for high latitude passive microwave snow water equivalent retrievals. J. Geophys. Res. 119, 7254–7270.

Dolant, C., Langlois, A., Montpetit, B., Brucker, L., Roy, A., Royer, A., 2016. Development of a rain-on-snow detection algorithm using passive microwave radiometry. Hydrol. Process. http://dx.doi.org/10.1002/hyp.10828 (13 pp.).

Gelman, A., Carlin, J.B., Stern, H.S., Rubin, D.B., 2014. Bayesian Data Analysis. third ed. Chapman & Hall/CRC Press, Boca Raton, FL.

Gilks, W.R., Roberts, G.O., Suhu, S.K., 1998. Adaptive Markov Chain Monte Carlo through regeneration. J. Am. Stat. Assoc. 93, 1045–1054.

Grenfell, T.C., Putkonen, J., 2008. A method for the detection of the severe rain-on-snow event on Banks Island, using passive microwave remote sensing. Water Resour. Res. 44, W03425. http://dx.doi.org/10.1029/2007WR005929.

Jenkins, D., 2007. Estimating Peary Caribou (*Rangifer tarandus pearyi*) and Muskox (*Ovibos moschatus*) Numbers, Composition and Distributions on Ellesmere Island, Nunavut. Interim Report. 2007.

Jenkins, D., Campbell, M., Hope, G., Goorts, J., McLoughlin, P., 2011. Recent Trends in Abundance of Peary Caribou (*Rangifer tarandus pearyi*) and Muskoxen (*Ovibos moschatus*) in the Canadian Arctic Archipelago, Nunavut. Department of Environment, Government of Nunavut, Wildlife Report No. 1, Pond Inlet, Nunavut, Canada.

Johnson, C.A., Neave, E., Blukacz-Richards, A., Banks, S.N., Quesnelle, P.E., 2016. Knowledge assessment (community and scientific) to inform the identification of critical habitat for Peary caribou, *Rangifer tarandus pearyi*, in the Canadian Arctic. Environment and Climate Change Canada, Science and Technology, Ottawa, Ontario, Canada.

Jolly, G.M., 1969. Sampling methods for aerial censuses of wildlife populations. East Afr. Agric. For. J. 34, 46–49.

Jones, P.D., Lister, D.H., Osborn, T.J., Harpham, C., Salmon, M., Morice, C.P., 2012. Hemispheric and large-scale land surface air temperature variations: an extensive revision and an update to 2010. J. Geophys. Res. 117, D05127.

Knowles, K., Njoku, E.G., Armstrong, R., Brodzik, M., 2000. Nimbus-7 SMMR Pathfinder Daily EASE-Grid Brightness Temperatures, Version 1. [Indicate Subset Used]. Boulder, Colorado USA. NASA National Snow and Ice Data Center Distributed Active Archive Center. http://dx.doi.org/10.5067/36SLCSCZU7N6 [Date Accessed].

Knowles, K., Savoie, M., Armstrong, R., Brodzik, M., 2006. AMSR-E/Aqua Daily EASE-Grid Brightness Temperatures, Version 1. [Indicate Subset Used]. Boulder, Colorado USA. NASA National Snow and Ice Data Center Distributed Active Archive Center. http://dx.doi.org/10.5067/XIMNXRTQVMOX [Date Accessed].

Kohler, J., Aanes, R., 2004. Effect of winter snow and ground icing on a Svalbard reindeer population: results of a simple snowpack model. Arct. Antarct. Alp. Res. 36, 333–341.

Krebs, C.J., 2001. Ecology: The Experimental Analysis of Distribution and Abundance. Fifth Edition. The University of British Columbia. Benjamin Cummings: An Imprint of Addison Wesley Longman, Inc., San Francisco, CA.

Langlois, A., Scharien, R., Geldsetzer, T., Iacozza, J., Barber, D.G., Yackel, J., 2008. Estimation of snow water equivalent over first-year sea ice using AMSR-E and surface observations. Remote Sens. Environ. 112, 3656–3667.

Larter, N.C., Nagy, J.A., 2001. Seasonal and annual variability in the quality of important forage plants on Banks Island, Canadian High Arctic. Appl. Veg. Sci. 4, 115–128.

Liebe, H.J., 1989. MPM - an atmospheric mm-wave propagation model. Int. J. Infrared Millimeter Waves 10, 631–650.

Liston, G.E., Hiemstra, C.A., 2011. The changing cryosphere: Pan-Arctic snow trends (1979–2009). J. Clim. 24, 5691–5712.

Liu, Y., Key, J.R., Liu, Z., Wang, X., Vavrus, S.J., 2012. A cloudier Arctic expected with diminishing sea ice. Geophys. Res. Lett. 39 (5 p).

Maslanik, J., Stroeve, J., 2004. DMSP SSM/I-SSMIS Daily Polar Gridded Brightness Temperatures, Version 4. [Indicate Subset Used]. Boulder, Colorado USA. NASA National Snow and Ice Data Center Distributed Active Archive Center. http://dx.doi.org/10.5067/AN9AI8EO7PX0 (Date Accessed 2016, updated 2016).

Mesinger, F., et al., 2006. North American regional reanalysis. Bull. Am. Meteorol. Soc. 87, 343–360.

Miller, F.L., 1986. An investigation of possible inter-island movements of Peary caribou across Prince of Wales Strait between Banks and Victoria Island. Northern Oil and Gas Program A12-1, Indian and Northern Affairs, Yellowknife, N.W.T.

Miller, F.L., Gunn, A., 2003. Catastrophic die-off of Peary caribou on the western Queen Elizabeth Islands, Canadian High Arctic. Arctic 56, 381–390.

Miller, F.L., Russell, R.H., Gunn, A., 1977. Interisland movements of Peary caribou (*Rangifer tarandus pearyi*) on western Queen Elizabeth Islands, arctic Canada. Can. J. Zool. 55, 1029–1037.

Miller, F., Edmonds, E.J., Gunn, A., 1982. Foraging behaviour of Peary caribou south of Viscount Melville Sound, Northwest Territories. Canadian Wildlife Service Progress Notes. 48 (41 p).

Miller, F.L., Barry, S.J., Calvert, W.A., 2005. Sea-ice crossings by caribou in the south-central Canadian arctic archipelago and their ecological importance. Rangifer 16, 77–88.

Montpetit, B., 2015. Analyse de la modélisation de l'émission multi-fréquences micro-onde des sols et de la neige, incluant les croutes de glace à l'aide du modèle Microwave Emission Model of Layered Snowpacks (MEMLS). (Ph.D. thesis). Université de Sherbrooke, Département de Géomatique Appliquée (May 2015, 188 p).

Montpetit, B., Royer, A., Roy, A., Langlois, A., Derksen, C., 2013. Snow microwave emission modeling of ice lenses within a snowpack using the Microwave Emission Model of Layered Snowpacks (MEMLS). IEEE Trans. Geosci. Remote Sens. 51, 4705–4717.

Ouellet, F., Langlois, A., Johnson, C.A., Richards, A., Royer, A., 2016. Spatialization of the SNOWPACK Snow Model in the Canadian Arctic for Peary Caribou Winter Grazing conditions Assessment. Submitted, Phys. Geogr. TPHY-2015-0077.

Papasodoro, C., Berthier, É., Royer, A., Zdanowicz, C., Langlois, A., 2015. Area, elevation and mass changes of the two southernmost ice caps of the Canadian Arctic Archipelago between 1952 and 2014. Cryosphere 9, 1535–1550.

Parker, G.R., Thomas, D.C., Broughton, E., Gray, D.R., 1975. Crashes of muskox and Peary caribou populations in 1973–74 on the Parry Islands, Arctic Canada. Canadian Wildlife Service Progress Notes. 56 (10 p).

Parkinson, C.L., 2014. Global sea ice coverage from satellite data: annual cycle and 35-yr trends. J. Clim. 27, 9377–9382.

Pulliainen, J., Grandell, J., Hallikainen, M., 1999. HUT snow emission model and its applicability to snow water equivalent retrieval. IEEE Trans. Geosci. Remote Sens. 37, 1378–1390.

Putkonen, J., Roe, G., 2003. Rain-on-snow events impact soil temperatures and affect ungulate survival. Geophys. Res. Lett. 30 (5 p).

Rees, A., Lemmetyinen, J., Derksen, C., Pulliainen, J., English, M., 2010. Observed and modelled effects of ice lens formation on passive microwave brightness temperatures over snow covered tundra. Remote Sens. Environ. 114, 116–126.

Rennert, K.J., Roe, G., Putkonen, J., Bitz, C.M., 2009. Soil thermal and ecological impacts of rain on snow events in the circumpolar Arctic. J. Clim. 22, 2302–2315.

Riseborough, D., Shiklomanov, N., Etzelmuller, B., Gruber, S., Marchenko, S., 2008. Recent advances in permafrost modelling. Permafr. Periglac. Process. 19, 137–156.

Romanovsky, V.E., Smith, S.L., Christiansen, H.H., 2010. Permafrost thermal state in the polar northern hemisphere during the international polar year 2007–2009: a synthesis. Permafr. Periglac. Process. 21, 106–116.

Roy, A., Royer, A., Wigneron, J.-P., Langlois, A., Bergeron, J., Cliche, P., 2012. A simple parameterization for a boreal forest radiative transfer model at microwave frequencies. Remote Sens. Environ. 124, 371–383.

Semmens, K.A., Ramage, J., Bartsch, A., Liston, G.E., 2013. Early snowmelt events: detection, distribution, and significance in a major sub-arctic watershed. Environ. Res. Lett. 8, 1–11.

Serreze, M.C., Barry, R.G., 2011. Processes and impacts of Arctic amplification: a research synthesis. Glob. Planet. Chang. 77, 85–96.

Serreze, M.C., Barrett, A.P., Stroeve, J.C., Kindig, D.N., Holland, M.M., 2009. The emergence of surface-based Arctic amplification. Cryosphere 3, 11–19.

Steele, M., Ermold, W., Zhang, J., 2008. Arctic ocean surface warming trends over the past 100 years. Geophys. Res. Lett. 35 (6 p).

Stien, A., Loe, L.E., Mysterud, A., Severinsen, T., Kohler, J., Langvatn, R., 2010. Icing events trigger range displacement in a high-arctic ungulate. Ecology 91, 915–920.

Vors, L.S., Boyce, M.S., 2009. Global declines of caribou and reindeer. Glob. Chang. Biol. 15, 2626–2633.

Weismüller, J., Wollschläger, U., Boike, J., Pan, X., Yu, Q., Roth, K., 2011. Modeling the thermal dynamics of the active layer at two contrasting permafrost sites on Svalbard and on the Tibetan Plateau. Cryosphere 5, 741–757.

Wiesmann, A., Mätzler, C., 1999. Microwave emission model of layered snowpacks. Remote Sens. Environ. 70, 307–316.

Winton, M., 2006. Does the Arctic sea ice have a tipping point? Geophys. Res. Lett. 33 (5 p).